APL Materials

Investigation of the effect of microstructural changes on thermal transport in semicrystalline polymer semiconductors

Cite as: APL Mater. 7, 081118 (2019); https://doi.org/10.1063/1.5111023
Submitted: 22 May 2019 . Accepted: 01 August 2019 . Published Online: 20 August 2019

Ekaterina Selezneva, Riccardo Di Pietro, Xuechen Jiao, Christopher R. McNeill, and Henning Sirringhaus

Investigation of the effect of microstructural changes on thermal transport in semicrystalline polymer semiconductors

Cite as: APL Mater. 7, 081118 (2019); doi: 10.1063/1.5111023
Submitted: 22 May 2019 • Accepted: 1 August 2019 •
Published Online: 20 August 2019

Ekaterina Selezneva,[1] Riccardo Di Pietro,[2] Xuechen Jiao,[3,4] Christopher R. McNeill,[3] and Henning Sirringhaus[1]

AFFILIATIONS

[1]Cavendish Laboratory, University of Cambridge, J J Thomson Avenue, CB3 0HE Cambridge, United Kingdom
[2]Hitachi Cambridge Laboratory, J J Thomson Avenue, CB3 0HE Cambridge, United Kingdom
[3]Department of Materials Science and Engineering, Monash University, Wellington Road, Clayton, Victoria 3800, Australia
[4]Australian Synchrotron, ANSTO, 800 Blackburn Road, Clayton, Victoria 3168, Australia

ABSTRACT

Great progress in the development of new semiconducting polymers over the last two decades alongside improved understanding of electron transport mechanisms have resulted in a dramatic increase in the electron mobility of these materials making them promising candidates for electronic and thermoelectric applications. Heat transport phenomena, on the other hand—which govern thermal conductivity—have not received as much attention up to date. In spite of the simplicity of the principle behind the measurement of thermoelectric properties, the combined uncertainty in thermoelectric figure of merit zT could easily reach 50% with the largest uncertainty coming from thermal conductivity measurements. Such a high measurement uncertainty, often comparable to relative variations in zT encountered when optimizing within a given class of materials, prevents the study of structure-thermal property relationships. Here we present a protocol for the measurement of the thermal conductivity of thin films with reduced measurement uncertainty, which allowed us to investigate the effect of microstructural changes on the thermal conductivity of the conjugated polymer P(NDI2OD-T2). We show that the enhancement of the thermal conductivity upon annealing is much less pronounced than the corresponding increase in the electron mobility that has been reported under the same annealing conditions in the literature. This suggests that semicrystalline conjugated polymers in which thermal transport remains limited by the amorphous domain boundaries in between crystalline grains could be a suitable system for realizing the electron-crystal phonon glass concept and enable higher performance thermoelectric materials.

INTRODUCTION

Current thermoelectric materials operate far from theoretical efficiency limits. There are intense ongoing research efforts to improve the efficiency of thermoelectric materials to enable wider applications in the harvesting of energy from waste heat. One class of materials being explored for this purpose are solution-processable organic semiconductors which could also offer routes to more cost-effective and scalable devices. However, in the past, their low electrical conductivity has created a bottleneck for adequate thermoelectric efficiency, preventing them from gaining practical significance.[1]

Great progress in polymer synthesis over the last two decades has led to development of high performance semiconducting polymers with electron mobility approaching that of amorphous silicon.[2] Many such high performance polymers self-order to form microcrystalline regions, with charge transport sensitive to film microstructure.

The efficiency of a thermoelectric material is determined by the dimensionless figure of merit $zT = S^2\sigma T/(\kappa_e + \kappa_{ph})$, where S is the Seebeck coefficient or thermopower, σ is electrical conductivity, $\kappa_e + \kappa_{ph}$ are the electronic and phononic components of thermal conductivity, respectively, and T is the absolute temperature. Although the thermoelectric performance of materials has

continuously improved over the last two decades, relative variations in zT encountered when optimizing within a given class of materials are small, i.e., typically not more than 15%–20%. At the same time, in spite of the measurement of thermoelectric properties being simple in principle, the combined uncertainty in zT could easily reach 50%,[3] with the largest uncertainty coming from thermal conductivity measurements. Accurate measurement of all transport coefficients and thermal conductivity, in particular, are thus essential for research of thermoelectric materials.

The thermal conductivity κ of a material is determined according to Fourier's law of heat conduction by measuring a temperature gradient across a sample in response to a known heat flux passing through it: $\dot{Q} = -\kappa\frac{\Delta T}{\Delta l}$, where $\dot{Q}$ is the heat flux passing through the sample, Δl is the sample length, and ΔT is the temperature difference across the sample.

Different from electrical conduction, heat conduction is virtually impossible to isolate solely using insulation.[4] In a typical thermal property measurement system, there will always be parasitic heat transfer present, such as radiative (infrared) heat exchange between instrument components and the environment or losses and thermal resistances at interfaces creating an uncertainty in the heat flux measured.[5] Another unexpectedly large uncertainty in thermal conductivity measurements comes from dimension measurements as has been demonstrated by an international round-robin testing of bulk thermoelectric materials.[6] According to internationally agreed guidelines on the measurement uncertainty, two types of errors are identified: systematic and random errors.[7–9] The systematic errors (affecting measurement accuracy) are those that remain constant in replicate measurements and are usually hard to identify and eliminate, whereas the random errors (affecting precision) are those that vary unpredictably in replicate measurements and responsible for the dispersion of results when replicate measurements are taken. In the case of thermal conductivity measurements, the former can be caused, for instance, by radiative heat exchange with environment, while the latter by variations in the interface thermal resistance.

The highest accuracy in thermal conductivity measurements (of the order 1%–5%) is achieved in the steady-state absolute guarded hot plate method,[10] which itself involves significant metrology and engineering challenges. Moreover, relatively large sample dimensions required for practical implementation of accurate temperature balancing and thermal contact resistances make the method not suitable for thin films, which are often of interest in the case of organic semiconductor samples. However, even when some sample characteristics, such as dimensions, limit substantially the measurement accuracy, high measurement reproducibility can still be achieved for a given measurement setup, allowing reliable material comparison. The scope of this work was thus to ensure sufficient measurement precision in thermal conductivity measurements on thin film conjugated polymers to enable confident investigations of how microstructural changes can influence their thermal conductivity contributing toward understanding mechanisms of the heat transport phenomena in semicrystalline polymer semiconductors.

Previously, Kommandur and Yee[11] reported the in-plane and through-plane thermal conductivities of poly(3-hexylthiophene), P3HT, and poly{[*N*,*N*-9-bis(2-octyldodecyl)naphthalene-1,4,5,8-bis(dicarboximide)-2,6-diyl]-*alt*-5,59-(2,29-bithiophene)}, P(NDI2OD-T2). The thermal conductivities were derived by using "classic" 3ω method in two different setup configurations: sample film on the substrate for the through-plane and the suspended film for the in-plane measurements. Comparisons of heat conduction in these different directions remain challenging, however, due to different boundary conditions of the two configurations. In the present work, we report an improved 3ω method that allows measurements with both higher accuracy and precision and has allowed us to detect changes in thermal conductivity upon crystallization of the conjugated polymer.

EXPERIMENTAL RESULTS

Material system

The microstructure of a typical semicrystalline conjugated polymer involves self-ordered structures of π-stacked polymer chains forming microcrystalline regions separated by amorphous phase. In face-on oriented systems, the direction of π-stacking is along the surface normal and the polymer chain direction and the direction of the solubilizing side chains is approximately in the plane [Fig. 1(a)]. In edge-on packed systems the direction of π-stacking is in plane. It has been reported previously that thermal annealing of semicrystalline polymers, especially those in the polythiophene family, such as P3HT and P(NDI2OD-T2), can result in microstructural changes including an increase in intracrystalline order and change in texture (such as the reorientation of face-on and edge-on crystalline domains).[12,13] In such model systems, these structural changes can be used to investigate the effect of morphology on thermal conductivity within the same sample. In this way, we ensure that the uncertainty associated with dimensional measurements eventually contributes only to a systematic error affecting measurement accuracy, but not the measurement precision and we can also eliminate the uncertainty coming from variations between the samples.

In this work, we focused on P(NDI2OD-T2) comparing thermal conductivity of the samples before and after annealing. The samples were spin-coated from 30 g/l dichlorobenzene (DCB) solution at the varying spin speed—for most films we used 1100 rpm resulting in the film thickness ~300 nm—and the films we dried in vacuum at room temperature. We refer to films prepared in this way as dry-cast (DC) below. The samples were then annealed for 30 min in inert atmosphere, first at 110 °C and then at 210 °C. At each stage, we performed thermal conductivity, thickness, and grazing incidence wide angle X-ray scattering (GIWAXS) measurements. In this temperature range, below the melting point, we only expected relatively subtle changes in the intracrystalline ordering that have been previously investigated.

Evolution of morphology upon thermal annealing

In order to characterize the evolution of morphology upon thermal annealing, we used grazing incidence wide angle X-ray scattering (GIWAXS) with varying angle of incidence. The 2D plots, obtained close to the critical angle and corresponding 1D profiles, are presented in Figs. 1(b) and 1(c), respectively. The results of the analysis are consistent with previously observed trends in P(NDI2OD-T2).[14–16] The films exhibit a predominantly face-on molecular packing, which was preserved after the annealing.

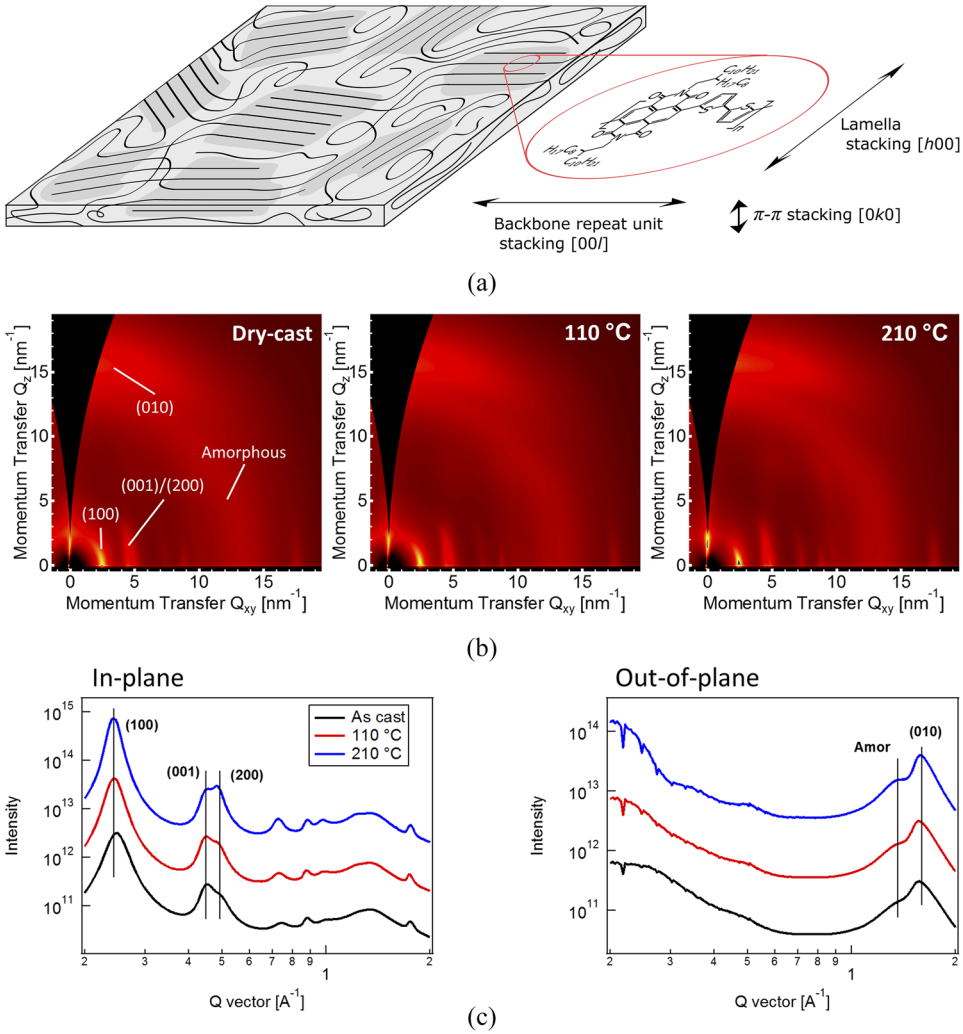

FIG. 1. (a) Schematic of face-on molecular packing of P(NDI2OD-T2) with shadowed regions highlighting ordered crystalline domains. The directions indicate crystallographic repeat units inferred from X-ray data. 2D plots (b) and 1D profiles (c) of grazing incidence wide angle X-ray scattering (GIWAXS) patterns of P(NDI2OD-T2) for dry-cast, annealed at 110 °C and annealed at 210 °C sample.

In addition, the spacing of lamellar, π-π, and backbone stacking did not change in a meaningful way along with annealing temperature. However, the coherence length of the in-plane lamellar stacking (200) reflection was found to increase with annealing from ~97 Å (DC) to 116 Å (annealed at 110 °C) and to 150 Å (annealed at 210 °C). Furthermore, the coherence length along the π-π direction was found to increase from ~35 Å (DC) to 37 Å (annealed at 110 °C) and to 42 Å (annealed at 210 °C). These observations indicate growth in the size of the crystallites along these crystallographic directions. On the other hand, the crystallite size along backbone stacking direction, (001), remained the same.

The ratio of the area of the (200) peak divided by the area of the (001) peak was found to gradually increase with increasing temperature, indicating that the lamellar crystallinity becomes enhanced compared to backbone crystallinity at higher annealing temperature. This observation confirms that the crystals tend to grow along the lamellar stacking and π-π stacking directions with annealing but not significantly along the backbone direction. Unfortunately, no reliable conclusion could be made regarding the fractional crystallinity of the polymer, as GIWAXS measurements of conjugated polymer films do not easily allow for determination of absolute degrees of crystallinity.

The depth resolved GIWAXS profiles (Fig. S1, supplementary material) obtained by varying the angle of incidence of the X-rays below the critical angle to achieve total external reflection with penetration depth of less than 10 nm indicated that trends in the bulk crystallinity hold throughout the whole film including the surface layer.

Thermal conductivity measurements

Thermal conductivity measurements were performed according to the 3ω-Völklein method[17,18] implemented in a commercial Linseis Thin Film Analyzer (TFA).[19] The uniqueness of the Völklein method is that it allows correction for heat losses associated with radiative heat transfer by estimating their contribution to the total

thermal conduction. This presents a powerful solution for thin films where sample dimensions do not allow practical implementation of thermal guarding, leaving no means to eliminate parasitic radiative losses via design of the experimental setup. In the Völklein method, two otherwise identical samples different only in geometry are measured. Since thermal conductance depends on thermal conductivity and emissivity, this allows for the solving of the system of two heat conduction equations deriving both coefficients.

In the Linseis TFA, a sample of interest is deposited (in this work spin-coated) on top of a silicon-based chip containing two free-standing high aspect ratio Si_3N_4 membranes of different areas. Each membrane contains a microfabricated wire aligned with the longitudinal axis that serves as a heater—creating a temperature gradient across the membrane—and a resistive thermometer. Effective heat sinking over the silicon rim isolates the two measurement areas of the sample film on top of the membranes. The high aspect ratio of the membranes (and hence of the effective sample areas) ensures that the heat flux is predominantly one-dimensional—in the plane of the membranes and perpendicular to the heater wires[20] [Fig. 2(a)]. Thus, the measurement probes the in-plane thermal conductivity of the sample, which is derived by a differential method. It involves subtracting the contribution from the empty membrane from the total thermal response of the membrane and sample.

Measurements of the thermal response of the system are based on the well-established 3ω method.[21] In this method, an AC current with frequency ω is applied to the heater wire connected in a 4-point-probe configuration. This results in the Joule heating of the membrane and the sample film, which is reflected in oscillations in the wire resistance at frequency 2ω. These resistance oscillations probed by the heating current at frequency ω produce a voltage component at frequency 3ω, which can be used to measure the temperature oscillations and thus the thermal response of the system. The temperature rise in a material is proportional to the thermal penetration depth defined as $d = \sqrt{\frac{D}{\pi f}}$, where D is the thermal diffusivity of the material, and f is frequency of the heat source. Thus, in the standard 3ω method, the measured temperature rise is used to derive the material's thermal diffusivity, while the thermal conductivity is derived indirectly using additional measurements of heat capacity C_p and material density ρ according to the following equation: $\kappa = D\rho C_p$. The uncertainty of the thermal conductivity value will thus have contributions from the uncertainties of the measurements of these physical quantities. It is worth pointing out that there can be significant uncertainties in the determination of both the sample density and the heat capacity. For instance, accurate heat capacity measurements are still very challenging: a variation of more than 15% was observed in the international round-robin study with all the laboratories following the same specific guide lines.[22] Different to the "classic" 3ω method, in the 3ω-Völklein method the heating is produced by applying a low frequency (0.4–0.5 Hz) AC current. Under these so-called "quasi steady-state" conditions, the heat penetrates through the whole sample volume and the measured temperature rise allows determination of the thermal conductivity directly according to Fourier's heat conduction equation without requiring measurement of C_p and ρ.

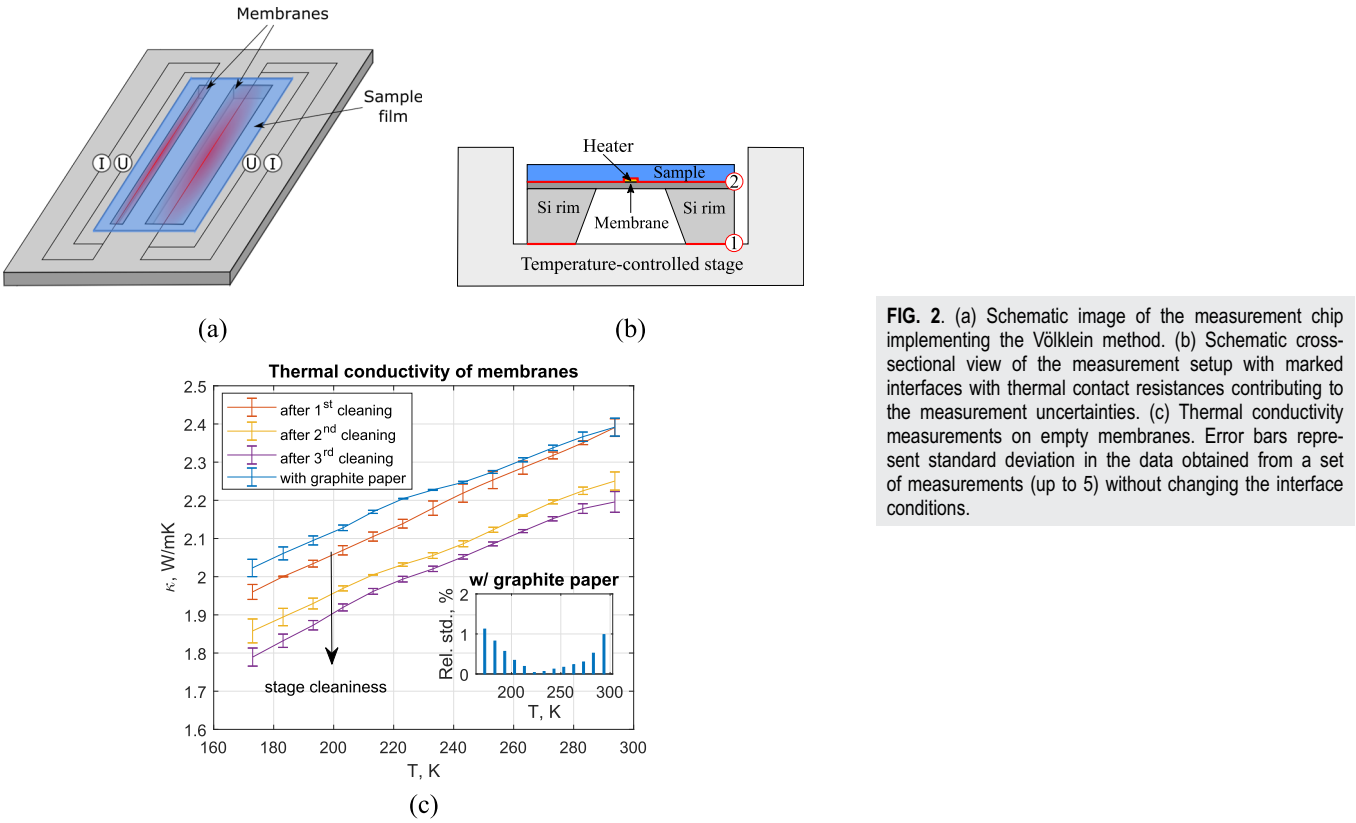

FIG. 2. (a) Schematic image of the measurement chip implementing the Völklein method. (b) Schematic cross-sectional view of the measurement setup with marked interfaces with thermal contact resistances contributing to the measurement uncertainties. (c) Thermal conductivity measurements on empty membranes. Error bars represent standard deviation in the data obtained from a set of measurements (up to 5) without changing the interface conditions.

Further experimental considerations to increase precision and accuracy of thermal conductivity measurements

Parasitic heat losses at the interfaces with thermal contact resistances are among the major sources of uncertainties in thermal conductivity measurements. In the Linseis TFA, there are two interfaces where thermal contact effects are most likely to arise: (1) between the measurement chip and the sample holder containing thermocouples used for the temperature control and the membrane heater wire calibration and (2) between the film and the membrane [interfaces marked as red lines in Fig. 2(b)].

Typically, the contribution from the thermal contact resistance at the interface (1) is minimized through improvement of the thermal contact by means of thermal interface materials, such as thermal paste. However, the homogeneity and amount of the thermal paste applied can seriously affect the repeatability of the measurement.[5] Indeed, in our experiments, we found out that even a small change in the amount of residual thermal paste at the interface (1) after sequential stage cleaning was affecting the measurement repeatability. The measurements were done on empty membranes after thermal paste removal. Each cleaning cycle resulted in further decrease of the thermal conductivity [Fig. 2(c)]. Residual thermal paste filling up micro-roughness features at the interface created a path for heat transfer. As the amount of residual paste decreased with sequential cleaning cycles, the thermal interface resistance increased, which reflected in the membrane heater wire calibration results and thus apparent thermal conductivity measured.

This issue has been resolved with the use of graphite paper (Panasonic, type EYG, 70 μm thick) as thermal interface material. The measurements showed high repeatability, which was not affected by graphite sheet replacements. The relative standard deviation between the measurements was <1.1% for the whole temperature range [Fig. 2(c), inset].

The contribution from the thermal contact resistance at the interface (2) can be estimated by plotting apparent thermal resistance, $R_{th} = \frac{\Delta T}{Q}$, with respect to the sample thickness and approximating the intercept of the trend with the y-axis. In this experiment, we varied the sample thickness via modulation of spin-coating speed from 500 to 1100 rpm with 200 rpm step, thus obtaining four samples of thickness in the range 300–600 nm. The thickness of each sample was estimated by taking an average of the average thicknesses extracted from Atomic Force Microscopy (AFM) topography scans at the sample edges in proximity of each of the four corners. All samples showed high uniformity in morphology (Fig. S2, supplementary material), while variation in thickness across the four AFM scans for each sample was <5%.

For accurate measurements, a relatively large sample thickness is needed in order to compensate for the polymer's relatively low thermal conductivity compared to that of the Si_3N_4 membrane and to ensure that the heat will not bypass the polymer sample via the less thermally resistive membrane. As can be seen in Fig. 3(a), summarizing data for DC samples (before thermal annealing) and the corresponding empty membranes, even for the thinnest sample spin-coated at 1100 rpm the total (sample + membrane) thermal resistance, were clearly separable from those of the empty membrane, indicating an evident contribution of the sample to the thermal response.

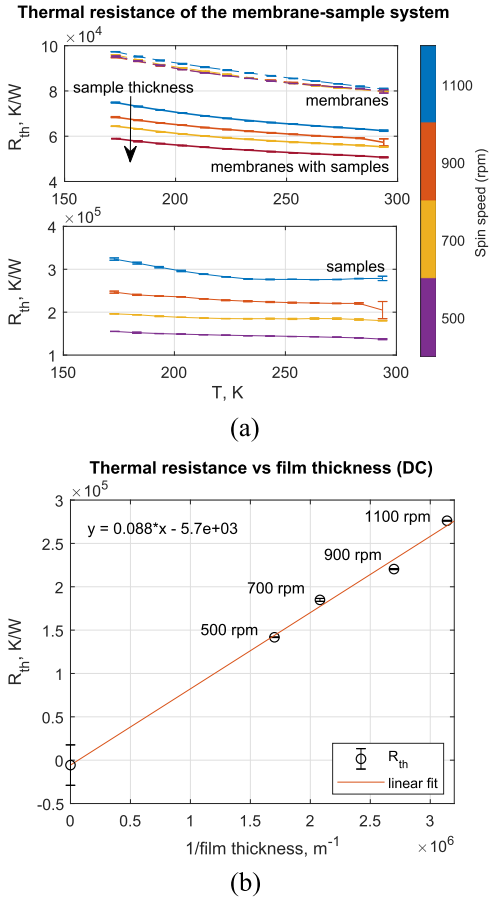

FIG. 3. (a) Measured thermal resistance of empty membranes and membranes with samples (top subplot) and derived thermal resistance of the samples (bottom subplot) for various sample thicknesses. (b) Thermal resistance of the sample as inverse function of its thickness. The intercept with y-axis is used to estimate the contribution from the thermal contact resistance at the interface (2). The corresponding error bar represents the standard error of the linear regression.

In Fig. 3(b), the thermal resistance of the sample is plotted vs inverse sample thickness. Note that the measurements were done in plane with the sample thickness defining the cross-sectional area for the heat transfer, not the length. Linear extrapolation of the intercept with y-axis resulted in negligibly small value ~2% of the magnitude of the sample thermal resistance with the thickness used in the present study. This value remained of the same order of magnitude and did not show a concurrent change upon annealing at 110 °C and 210 °C. However, a large standard error on the intercept (~8% of the magnitude of the sample thermal resistance) did not allow us to determine the thermal contact resistance with high precision. Nevertheless, within the determined confidence interval, it is reasonable to conclude that the thermal contact resistance at the interface (2) does not dominate the apparent thermal conductivity.

Another source of the apparent thermal contact resistance value may come from the measurement artifact caused by slight cold side temperature rise that is assumed to be at the temperature

of the silicon rim. However, based on calculation in Ref. 20, for a given sample thermal conductivity range and thickness, the estimated uncertainty is expected to be <0.9%. This value is significantly lower the linear regression error and thus can be considered negligible.

Evolution of thermal conductivity upon thermal annealing

Previous studies of charge transport of P(NDI2OD-T2) revealed a 3-fold increase in electron mobility upon annealing under the conditions used here which was correlated with an increase of grain size and the degree of crystallinity.[14–16] In semiconducting polymers, the contributions from both electrons and phonons to the thermal conductivity should be considered. The electronic component of thermal conductivity is expected to follow electrical conductivity according to the Wiedemann-Franz law. Phonons, on the other hand, have different (usually larger) mean free path than that of electrons and thus may experience different scattering mechanisms. The samples under investigation were undoped; thus, the electronic contribution to the heat transport could be neglected and the thermal conductivity measurements could be used to investigate the effect of increased degree of crystallinity on phonon transport.

The obtained thermal conductivity data are summarized in Fig. 4. The temperature dependence of the thermal conductivity for each sample state (DC, annealed at 110 °C, annealed at 210 °C) showed a concurrent increase with temperature found in glasses and in a range of disordered crystals.[23] In such systems, strong phonon damping above ~30 K results in localized lattice vibrations which are more appropriate to describe via the Einstein model of isolated atomic oscillations[24] with the heat being carried out through the lattice by a random walk rather than by wavelike motion of collective oscillations of the Debye and Born-von Karman models.[25,26] Localized oscillations with the mean free path approaching interatomic spacing—the shortest wavelength possible in solid—become insensitive to the common phonon scattering mechanisms (grain boundary scattering, Umklapp phonon-phonon scattering, lattice defects

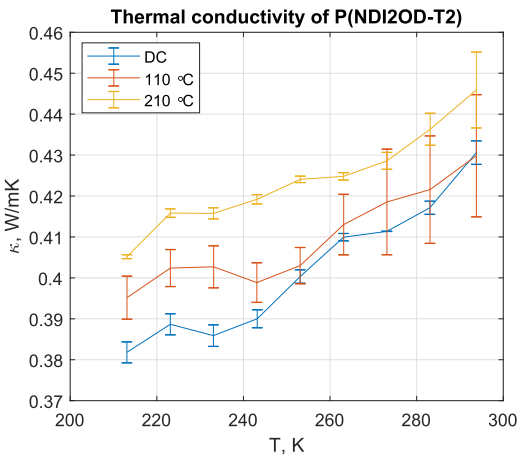

FIG. 4. Thermal conductivity evolution of P(NDI2OD-T2) upon thermal annealing.

scattering, etc.) responsible for the decrease in thermal conductivity with increasing temperature observed in crystalline materials (Ref. 27 and references therein).

The absolute value of the in-plane thermal conductivity at ambient temperature for the DC samples is ~60% higher than the in-plane thermal conductivity reported for this material by Kommandur and Yee[11] and ~15% lower the in-plane thermal conductivity of poly(3,4-ethylenedioxythiophene) (PEDOT) reported by Liu *et al.*[28] The value is nearly double the cross-plane thermal conductivity reported by Duda *et al.*[29] for PEDOT and P3HT and three times the thermal conductivity of polypyromellitimide: (PPMI) quoted by manufacturer.[30]

Upon annealing the films at 210 °C, we observed a small increase in thermal conductivity by 5.4% ± 1.8% averaged over the measured temperature range compared to the DC samples (before thermal annealing).

This effect cannot be attributed to any sample degradation or doping of the polymer. Doping could, in principle, increase the carrier concentration and induce an electronic component of the thermal conductivity. However, P(NDI2OD-T2) is an n-type polymer and is unlikely to be doped when stored in air. Furthermore, all measurements were performed within three days, a period over which no changes in thermal conductivity were observed when remeasuring an unprocessed (DC) sample. The sample thickness was measured at each stage, and no change has been detected upon thermal annealing.

The small increase in the thermal conductivity may be considered statistically insignificant in view of larger uncertainty in the thermal contact resistance at the interface (2). However, eventual possible change in thermal conductivity within the determined confidence interval is nevertheless small. This finding indicates that in contrast to charge transport, which is improved significantly over this range of annealing temperature with electron mobility enhanced by a factor of 3,[14–16] increased crystallinity did not have such a dramatic effect on thermal transport. This is furthermore surprising considering the studies on polycrystalline polyethylene which revealed an over 3-fold increase in thermal conductivity with increasing crystallinity level from 44% to 98%.[31] This result can be understood by considering the microstructure of semicrystalline polymer semiconductors, which comprise crystalline domains separated by an amorphous phase. For sufficiently large fraction of crystalline phase, long tie chains in amorphous regions interconnect the crystallites, which creates a network for efficient charge transport.[32] Thermal annealing promotes intracrystalline ordering and crystallite growth enhancing phonon transport in the crystalline phase through reduced phonon scattering on defects and crystallites grain boundaries. However, the amorphous phase still presents an efficient scattering medium for the phonon transport, resulting in very modest net increase in the phononic component of thermal conductivity.

This finding is especially significant and beneficial for a thermoelectric material as it suggests that since increased crystallinity while dramatically improving electron mobility can have a very modest effect on the phononic component of thermal conductivity. This implies that it might be possible to decouple electron and phonon transport in semicrystalline semiconducting polymer systems and realize the so-called "phonon glass-electron crystal"[33] requirement. In inorganic materials, electron and phonon transport are typically

interconnected, which often presents a significant obstacle for the thermoelectric optimization.

SUMMARY

In view of large combined uncertainty in the measurements of thermoelectric figure of merit, with the largest contribution coming from thermal conductivity measurements, great care must be taken for all transport coefficients measurements and thermal conductivity in particular. Following a protocol for thermal conductivity measurements of thin films with reduced measurement uncertainty we have investigated the effect of microstructural changes on the thermal conductivity of P(NDI2OD-T2). Upon annealing films at 210 °C, we observed a significant, but small increase in thermal conductivity of 5.4% ± 1.8% compared to samples prepared without thermal annealing. This increase is at the limit of what can be considered statistically significant if we take into account the uncertainty in determining the thermal contact resistance. In any case, the change in thermal conductivity is nevertheless much smaller compared to the ensuing improvement in charge transport mobility. One possible explanation for this discrepancy that the amorphous phase still presents an efficient scattering medium for the phonon transport resulting in only a very modest net increase in the phononic component of thermal conductivity. This finding is especially significant and beneficial for a thermoelectric material as it suggests that since increased crystallinity, while dramatically improving electron mobility, had a very modest effect on the phononic component of the thermal conductivity, it might be possible to decouple electron and phonon transport in semicrystalline semiconducting polymer systems and realize the so-called "phonon glass-electron crystal" concept.

SUPPLEMENTARY MATERIAL

See supplementary material for the depth-resolved GIWAXS profiles of P(NDI2OD-T2) and representative AFM images used to determine the samples thicknesses.

ACKNOWLEDGMENTS

This work was performed in part at the SAXS/WAXS beamline at the Australian Synchrotron, part of ANSTO. We gratefully acknowledge funding from the Centre for Advanced Materials for Integrated Energy Systems (CAMIES, Grant No. EP/P007767/1).

REFERENCES

[1] B. Russ *et al.*, Nat. Rev. Mater. **1**, 16050 (2016).
[2] H. Sirringhaus *et al.*, Science **280**, 1741 (1998).
[3] G. J. Snyder and E. S. Toberer, Nat. Mater. **7**, 105 (2008).
[4] E. Selezneva *et al.*, *Energy and Environment Series* (RSC, 2016), p. 17.
[5] P. D. Chao *et al.*, Meas. Sci. Technol. **27**, 085002 (2016).
[6] H. Wang *et al.*, J. Electron. Mater. **42**, 654 (2013).
[7] Joint Committee for Guides in Metrology (JCGM), *Evaluation of Measurement Data–Guide to the Expression of Uncertainty in Measurement (GUM)* (International Organization for Standardization, Geneva, 2008).
[8] United Kingdom Accreditation Service (UKAS), *The Expression of Uncertainty and Confidence in Measurement* (United Kingdom Accreditation Service, 2012).
[9] S. Bell, *Good Practice Guide No. 11: A Beginner's Guide to Uncertainty of Measurement* (National Physical Laboratory, UK, 1999).
[10] ASTM-C177, Standard Test Method for Steady-State Heat Flux Measurements and Thermal Transmission Properties by Means of the Guarded-Hot-Plate, ASTM-C177, 2013.
[11] S. Kommandur and S. Yee, Rev. Sci. Instrum. **89**, 114905 (2018).
[12] E. Verploegen *et al.*, Adv. Funct. Mater. **20**, 3519 (2010).
[13] J. Rivnay *et al.*, Macromolecules **44**, 5246 (2011).
[14] R. Steyrleuthner *et al.*, J. Am. Chem. Soc. **136**, 4245 (2014).
[15] R. Di Pietro *et al.*, Adv. Funct. Mater. **26**, 8011 (2016).
[16] M. Statz *et al.*, Commun. Phys. **1**, 16 (2018).
[17] F. Völklein *et al.*, Phys. Status Solidi A **210**, 106 (2013).
[18] A. Sikora *et al.*, Rev. Sci. Instrum. **83**, 054902 (2012).
[19] V. Linseis *et al.*, Rev. Sci. Instrum. **89**, 015110 (2018).
[20] V. Linseis *et al.*, J. Electron. Mater. **47**, 3203 (2018).
[21] D. G. Cahill and R. O. Pohl, Phys. Rev. B **35**, 4067 (1987).
[22] H. Wang *et al.*, J. Electron. Mater. **42**, 1073 (2013).
[23] D. Cahill *et al.*, Phys. Rev. B **46**, 6131 (1992).
[24] A. Einstein, Ann. Phys. **35**, 679 (1911).
[25] P. Debye, Ann. Phys. **39**, 789 (1912).
[26] M. Born and T. von Karman, Phys. Z. **13**, 297 (1912).
[27] D. Cahill and R. Pohl, Annu. Rev. Phys. Chem. **39**, 93 (1988).
[28] J. Liu *et al.*, Macromolecules **48**, 585 (2015).
[29] J. C. Duda *et al.*, Appl. Phys. Lett. **102**, 251912 (2013).
[30] See https://www.dupont.com/content/dam/dupont/products-and-services/membranes-and-films/polyimde-films/documents/DEC-Kapton-summary-of-properties.pdf for Dupont Kapton Summary of Properties.
[31] I. Engeln and M. Meissner, "Thermal properties of crystalline polymers at low temperatures," in *Nonmetallic Materials and Composites at Low Temperatures*, edited by G. Hartwig *et al.* (Plenum Press, New York, 1982).
[32] R. Noriega *et al.*, Nat. Mater. **12**, 1038 (2013).
[33] *CRC Handbook of Thermoelectrics*, edited by D. M. Rowe (CRC Press, Bota Raton, 1995).